Effect of Strain on Charge Density Wave Order in the Holstein Model

B. Cohen-Stead,[1] N.C. Costa,[2] E. Khatami,[3] and R.T. Scalettar[1]

[1] *Department of Physics, University of California, Davis, CA 95616,USA**

[2] *Instituto de Física, Universidade Federal do Rio de Janeiro Cx.P. 68.528, 21941-972 Rio de Janeiro RJ, Brazil*

[3] *Department of Physics and Astronomy, 1 Washington Square, Science Building 148, San Jose, CA 95192*

(Dated: January 2, 2019)

We investigate charge ordering in the Holstein model in the presence of anisotropic hopping, $t_x, t_y = 1-\delta, 1+\delta$. Using Quantum Monte Carlo simulations, we show that density correlations are relatively insensitive to moderate anisotropy $\delta \lesssim 0.15$, but begin to decrease rapidly at fixed temperature T for $\delta \sim 0.30$. Accompanying Mean Field Theory calculations show a similar qualitative structure, with T_c relatively constant at small δ and then decreasing much more rapidly at $\delta \sim 0.40$. We also obtain the density of states $N(\omega)$ and the momentum-dependent spectral function, $A(\mathbf{p}, \omega)$. The density of states provides a more clear signal of the charge ordering transition T_c at large strain δ than does finite size scaling of the charge structure factor because of the small value of the order parameter.

PACS numbers: 71.10.Fd, 71.30.+h, 71.45.Lr, 74.20.-z, 02.70.Uu

INTRODUCTION

Introduction needs to be smoothed out.

Studies of the effect of strain on charge density wave (CDW) materials have seen a significant rise in activity in the past several years[1–3]. The general interest originates from the ability to tune a strongly correlated insulating phase and induce transitions into alternate patterns of charge order, or into metallic and even superconducting phases. The application of strain also provides specific insight into the nature of the native CDW phase, for example into the role of Fermi surface nesting[4, 5], by altering the band structure. Layered transition metal dichalcogenides (TMDs) are one of the most commonly investigated classes of CDW materials; their transitions have previously been tuned by varying the thickness or gate potential[6–11]. In $2H$-$NbSe_2$ the CDW transition temperature T_c increases from $T_c = 33$ K in the bulk to $T_c = 145$ K in a single layer[12]. A similar, albeit much smaller, effect is seen in $1T$-$TiSe_2$[13, 14]. Strain is therefore useful since it provides an alternate method for modulating CDW physics. Indeed, the exploration the potential use of strain to adjust optical, magnetic and conductivity properties, especially in TMDs, has been referred to as 'strain engineering'.

Much of the existing theoretical work in the area has been within first-principles density functional theory (DFT). These studies find that, for $1T$-$TiSe_2$ the CDW transition temperature can be enhanced or suppressed with the application tensile or compressive strain, respectively[2]. In the latter case, the weakened CDW opens the door for superconductivity (SC). This contrasting behavior is linked to the distinct behavior of the band gap upon extension versus compression. Strain has been shown to enhance SC in Na-intercalated $NbSe_2$ as well[15]. Initially, the Na intercalation creates a large electron doping which contracts the Fermi surface and causes CDW to disappear. The subsequent application of strain increases the density of states at the Fermi surface and more than doubles the SC T_c.

CDW materials, including the TMDs, generally have rich (e.g. layered) structures. The charge ordering may not be commensurate with the lattice, and may also differ on the surface and within the bulk. The application of strain has additional complicating effects, including changes in the phonon spectrum and of the relative placement of different orbitals (energy bands). $1T$-VSe_2 in particular has a transition from hexagonal to rectangular charge order wth strain which seems to originate in the softening of certain phonon modes with strain[16]. The aforementioned DFT investigations have explored many of these details.

An alternate theoretical approach to DFT which lends insight into CDW physics is through the solution of simple model Hamiltonians. These can treat intersite electron-electron interactions V, as described, for example, by the extended Hubbard model. Charge order arises directly from the minimization of the intersite repulsion energy V by alternating empty and occupied sites. Alternately, one can focus on electron-phonon interactions, such as those incorporated in the Holstein[17] or Su-Schrieffer-Heeger[18] models. Here the driving force for CDW formation is a lowering of the electron kinetic energy through the opening of a gap in the spectrum. This energy lowering competes with the cost in elastic energy associated with displacing the phonon positions.

Investigation of quasi-2D materials, and on surfaces motivates the theoretical study of two dimensional geometries. Here, we focus on a simple model of charge order driven by electron-phonon interactions, the square lattice Holstein model. We incorporate the most direct effect of strain, the enhancement of the orbital overlap integral by compression, through an anisotropy in the

hopping in the x and y directions. Our model is,

$$\begin{aligned}\hat{\mathcal{H}} = &- t_x \sum_{\mathbf{i},\sigma} \left(\hat{d}^\dagger_{\mathbf{i},\sigma} \hat{d}_{\mathbf{i}+\hat{x},\sigma} + \hat{d}^\dagger_{\mathbf{i}+\hat{x},\sigma} \hat{d}_{\mathbf{i},\sigma} \right) \\ &- t_y \sum_{\mathbf{i},\sigma} \left(\hat{d}^\dagger_{\mathbf{i},\sigma} \hat{d}_{\mathbf{i}+\hat{y},\sigma} + \hat{d}^\dagger_{\mathbf{i}+\hat{y},\sigma} \hat{d}_{\mathbf{i},\sigma} \right) - \mu \sum_{\mathbf{i},\sigma} \hat{n}_{\mathbf{i},\sigma} \\ &+ \frac{1}{2} \sum_{\mathbf{i}} \hat{P}^2_{\mathbf{i}} + \frac{\omega_0^2}{2} \sum_{\mathbf{i}} \hat{X}^2_{\mathbf{i}} + \lambda \sum_{\mathbf{i},\sigma} \hat{n}_{\mathbf{i},\sigma} \hat{X}_{\mathbf{i}} \ . \end{aligned} \tag{1}$$

Here $\hat{d}^\dagger_{\mathbf{i},\sigma}(\hat{d}_{\mathbf{i},\sigma})$ are creation(destruction) operators for a fermion of spin $\sigma =\uparrow,\downarrow$ at site $\mathbf{i}$ of a two dimensional square lattice. Thus the first term represents an electron kinetic energy (band structure) with hoppings t_x, t_y and dispersion $\epsilon_{\mathbf{p}} = -2t_x \cos p_x - 2t_y \cos p_y$. $\hat{P}_{\mathbf{i}}$ and $\hat{X}_{\mathbf{i}}$ describe a local phonon mode of frequency ω_0 on site $\mathbf{i}$. The electron-phonon coupling λ connects the electron density $\hat{n}_{\mathbf{i}} = \hat{n}_{\mathbf{i},\uparrow} + \hat{n}_{\mathbf{i},\downarrow}$ at site $\mathbf{i}$ with the displacement $\hat{X}_{\mathbf{i}}$.

At constant volume, compression along one axis is accompanied by an expansion in the orthogonal direction. In what follows we set $t_x = 1-\delta$ and $t_y = 1+\delta$, a choice which keeps $t_x + t_y = 2$, and hence the bandwidth $W = 4(t_x + t_y)$ constant. This choice is motivated physically by the remarks above, but also allows us to separate the effect of hopping anisotropy from changes which would accompany a simple isotropic reduction or enhancement of W.

The electron-phonon interaction promotes local pairing of electrons. This can easily be seen by considering the single site ($t = 0$) limit. Integrating out the phonon degrees of freedom leads to an effective attraction between the up and down spin fermions $U_{\text{eff}}\, n_{\mathbf{i},\uparrow} n_{\mathbf{i},\downarrow}$, with $U_{\text{eff}} = -\lambda^2/\omega_0^2$. Associated with this attraction is an oscillator displacement $x_* = -\lambda \langle n \rangle / \omega_0^2$.

At strong coupling, well formed local pairs form due to this on-site attraction. These pairs prefer to organize their placements spatially. In particular, as the density approaches half-filling, $\langle n \rangle = 1$, on a bipartite lattice, electron pairs and empty sites alternate on the two sublattices. This CDW pattern is favored energetically because the energy of neighboring occupied and empty sites is lower by t^2/U_{eff} relative to two adjacent occupied or empty sites. This argument closely parallel the one which motivates the appearance of antiferromagnetic (AF) order in the large U (Heisenberg) limit of the half-filled repulsive Hubbard model, where well-formed local moments of up and down spin alternate due to the $J \sim t^2/U$ lowering of the energy relative to parallel spin placement.

There is a similar analogy between the Hubbard and Holstein Hamiltonians at weak coupling. In the Hubbard model at $U \lesssim t$, AF order is associated with Fermi surface nesting and a 'Slater insulating' phase- the opening of an AF gap lowers the electron kinetic energy. In the Holstein model, an alternation of phonon displacements opens a CDW gap, with similar effect. It is interesting that these close analogies exist despite the fact that the Holstein Hamiltonian has a second set of (phonon) degrees of freedom which is absent in the Hubbard Hamiltonian.

MEAN FIELD THEORY

We first solve Eq. 1 within a simple mean field approach by ignoring the phonon kinetic energy and making the *ansatz* $\hat{X}_{\mathbf{i}} \to x_0 + (-1)^{\mathbf{i}} x_1$. The value x_0 describes a site-independent phonon displacement of the similar to that described in the preceding section, while x_1 is the CDW order parameter, a nonzero value breaking the symmetry between the two (equivalent) sublattices. Ben- is x_0 the same value as x_* previously (from $t = 0$ calculation)? It is not obvious to me that turning on t should not affect the uniform displacement. Perhaps it is a particle-hole symmetry thing?

Inserting this form into Eq. 1, the quadratic Hamiltonian can be diagonalized. From the resulting electronic energy levels E_α one can compute the free energy as a function of the order parameter x_1,

$$F(x_1) = \frac{N}{4}\omega_0^2 x_1^2 - 2T \sum_\alpha \ln\left(1 + e^{-\beta E_\alpha(x_1)}\right) \tag{2}$$

Minimizing $F(x_1)$ determines the presence (x_1 nonzero) or absence ($x_1 = 0$) of CDW order: Since the product of the electron-phonon coupling λ and the phonon displacement $x_{\mathbf{i}}$ represents a local site energy, associated with a non-zero value of x_1 will be a CDW alternation.

Equivalently, one can write down coupled self-consistent equations: Given x_0, x_1, the (quadratic) Hamiltonian is diagonalized and the resulting charge densities $n_{\mathbf{i}} = n + (-1)^{\mathbf{i}} \nu$ are computed. From these, x_0 and x_1 are updated via $x_0 = (-2\lambda^2/\omega_0^2)\, n$ and $x_1 = (-2\lambda^2/\omega_0^2)\, \nu$. This process is iterated to convergence.

Ben- please verify this discussion, e.g. factors of two immediately above seem inconsistent with earlier text?

The change of variables to $y = \omega_0 x$ makes it evident that within MFT the behavior of the Holstein model is governed only by the combination λ^2/ω_0^2 rather than on λ and ω_0 individually. (This is only approximately true in exact solutions, e.g. within DQMC.) We therefore define the dimensionless coupling constant $\lambda_D \equiv \lambda^2/(\omega_0^2\, W)$ where $W = 8$ is the fermion bandwidth, and present results as functions of λ_D.

We can easily generate many MFT results. The captions to the figure placeholders indicate some possible things we could show. I am by no means wedded to these choices. Whatever you think is most interesting. These MFT results need to be described here in the text, but I will not do so because we have not decided what they are.

One point we might want to make in the figures is the smallness of the order parameter at large δt. This will

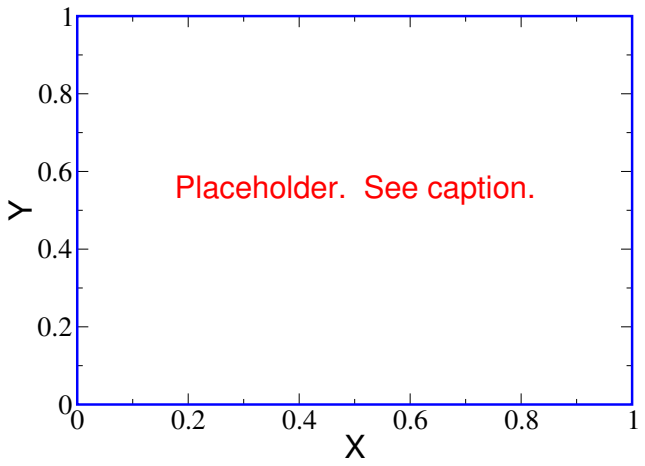

FIG. 1. MFT result #1 The staggered phonon displacement x_1 is shown as a function of temperature T for different values of the hopping anisotropy δ. Here the lattice size is N = 10x10, and the dimensionless coupling λ_D =?? (just one?). x_1 onsets with the usual MFT order parameter critical exponents β at the transition temperature T_c.

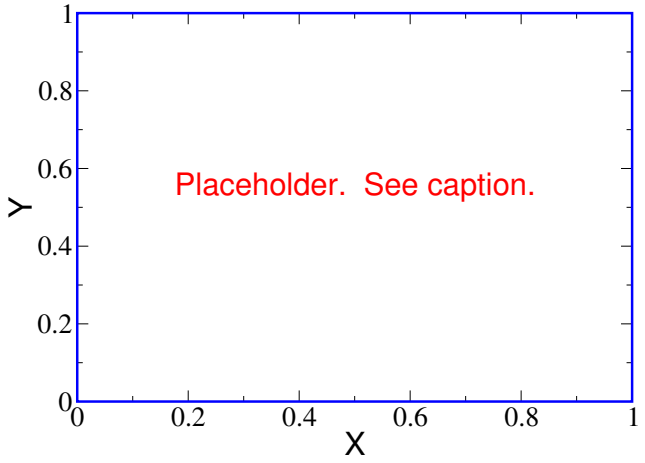

FIG. 2. MFT result #2 The staggered charge density ν as a function of the phonon order parameter x_1 for different δ. Here the lattice size is N = 10x10, and the dimensionless coupling λ_D =?? (just one?).

connect with why it is hard to see CDW order in DQMC by studying $S_{\rm cdw}$.

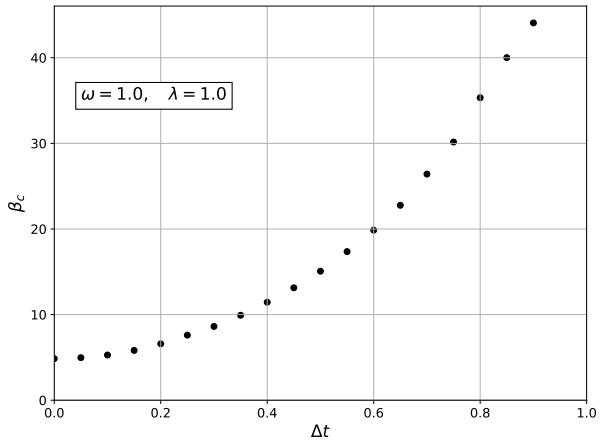

FIG. 3. MFT result #3; preliminary version from Ben. Critical inverse temperature β_c for the CDW transition versus hopping anisotropy δ. Results for several values of the dimensionless electron-phonon coupling λ_D are shown.

QUANTUM MONTE CARLO

Methodology

We next treat the Hamiltonian Eq. 1 with determinant Quantum Monte Carlo. The inverse temperature β is discretized into L intervals of length $\Delta\tau$. Complete sets of phonon position eigenstates $\{x_{\mathbf{i}}(\tau)\}$ are then introduced between each incremental imaginary time evolution operator $e^{-\Delta\tau\hat{\mathcal{H}}}$. This leads to the usual "bosonic' action of the quantum harmonic oscillator

$$S_{\rm bose} = \Delta\tau\Big(\frac{1}{2}\omega_0^2\sum_{\mathbf{i}} x_{\mathbf{i}}(\tau)^2 + \frac{1}{2}\sum_{\mathbf{i}}\big(\frac{x_{\mathbf{i}}(\tau) - x_{\mathbf{i}}(\tau)}{\Delta\tau}\big)^2\Big) \tag{3}$$

The fermionic operators appear only quadratically, and can be traced out analytically. The result is the product of the determinants of two matrices M_σ, one each for spin $\uparrow,\downarrow$. The remaining trace over the phonon field involves a sum over the classical variables $x_{\mathbf{i}}(\tau)$ indexed by the two spatial and one imaginary time direction. This is done via monte carlo sampling.

Because the two spin species couple in the same way to the phonon coordinates, the matrices are identical. Hence the product of their determinants, which gives the weight of the configuration $\{x_{\mathbf{i}}(\tau)\}$, is always positive. There is no 'sign problem'[19, 20] at any value of the Hamiltonian parameters, temperature or density. (Nevertheless, we limit the studies to be reported here to half-filling $\rho_\sigma = \langle n_{\mathbf{i}\sigma}\rangle = \frac{1}{2}$.)

Should we show MFT results away from half-filling?

The principle limitations of DQMC, as with most monte carlo simulations, are finite lattice sizes and statistical error bars on the observables. ($\Delta\tau$ is chosen

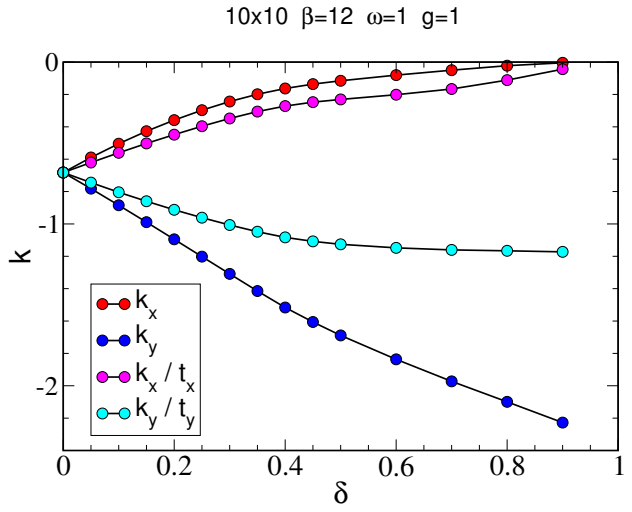

FIG. 4. The electron kinetic energies k_x and k_y are shown as a function of δ. Division by the energy scales t_x and t_y isolates the effect of anisotropy on the hopping.

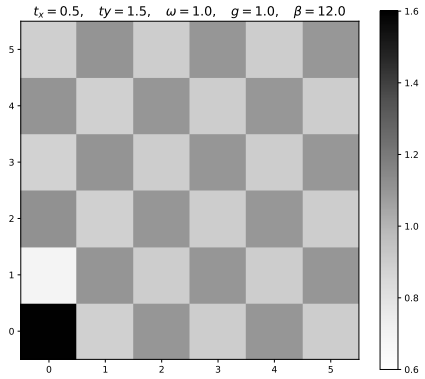

FIG. 5. Real space spin correlations for a moderately strained lattice, $t_x = 0.5$, $t_y = 1.5$. The phonon frequency $\omega_0 = t$ and electron phonon coupling $g = t$. Temperature $T = t/12$. The oscillating checkerboard charge density pattern persists across the entire 8x8 lattice. preliminary

small enough so that Trotter errors associated with the discretization of β are smaller than the statistical ones.) One way in which finite size errors manifest in DQMC is via the discrete set of momentum points $\{\mathbf{p}\}$. Here we use antiperiodic boundary conditions for lattice sizes 6×6 and 10×10, and periodic boundary conditions for 4×4 and 8×8. This keeps the proportion of $\mathbf{p}$ points directly on the Fermi Surface the same for all lattice sizes.

DQMC can access a wide variety of observables, since expectation values of fermionic operators are easily expressed in terms of matrix elements of $G = M^{-1}$ and their products. Here we focus on the kinetic energies in

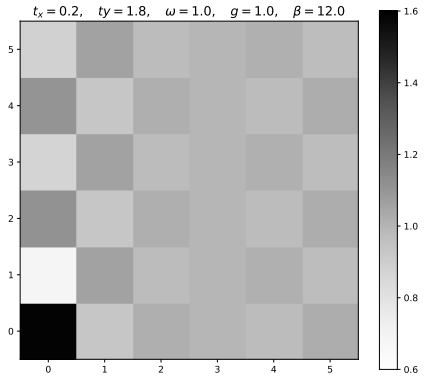

FIG. 6. Real space spin correlations for a highly strained lattice, $t_x = 0.2$, $t_y = 1.8$. The phonon frequency $\omega_0 = t$ and electron phonon coupling $g = t$. Temperature $T = t/12$. The oscillating checkerboard charge density pattern persists in the $\hat{y}$ direction only, with a pair of vertical domain wall along $y = 3$ and $y = 7$ across which the sublattices with large and small density interchange. lattice. preliminary

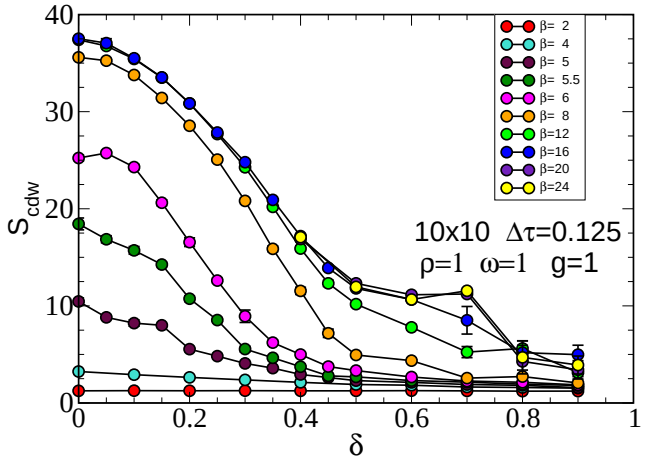

FIG. 7. CDW structure factor versus hopping anisotropy δ. For small δ there is a rapid growth in $S_{\rm cdw}$ near the CDW $\beta_c \approx 6/t$. For $\delta \gtrsim 0.5$ this growth becomes less evident. Either a CDW transition does not occur, or else its critical temperature is below those simulated. This plot needs improvement. I am running more realizations for $\beta = 12, 16, 20, 24$.

the x and y directions,

$$k_x \equiv \Big\langle -t_x \sum_\sigma \big(\hat{d}^\dagger_{\mathbf{i},\sigma} \hat{d}^\dagger_{\mathbf{i}+\hat{x},\sigma} + \hat{d}^\dagger_{\mathbf{i}+\hat{x},\sigma} \hat{d}^\dagger_{\mathbf{i}+\hat{x},\sigma} \big) \Big\rangle$$
$$k_y \equiv \Big\langle -t_y \sum_\sigma \big(\hat{d}^\dagger_{\mathbf{i},\sigma} \hat{d}^\dagger_{\mathbf{i}+\hat{y},\sigma} + \hat{d}^\dagger_{\mathbf{i}+\hat{y},\sigma} \hat{d}^\dagger_{\mathbf{i},\sigma} \big) \Big\rangle \qquad (4)$$

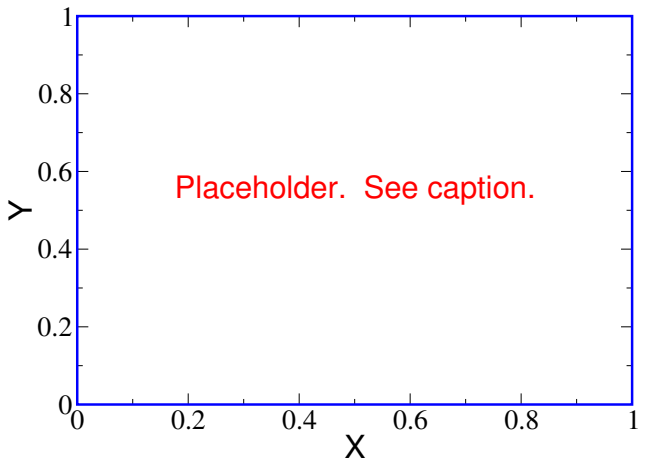

FIG. 8. Finite size scaling analysis of the structure factor is shown for $\delta t = 0.4$. At left, $S_{\rm cdw}$ as a function of β for different lattice sizes. At right, the scaled form $L^{-7/4} S_{\rm cdw}$ shows a crossing which determines β_c.

and on the CDW structure factor

$$S_{\rm cdw} = \langle \frac{1}{N} \sum_{\mathbf{i},\mathbf{j}} \left(n_{\mathbf{i}\uparrow} + n_{\mathbf{i}\downarrow} \right) \left(n_{\mathbf{j}\uparrow} + n_{\mathbf{j}\downarrow} \right) \rangle (-1)^{\mathbf{i}+\mathbf{j}} \quad (5)$$

where $(-1)^{\mathbf{i}+\mathbf{j}} = +1(-1)$ for sites $\mathbf{i},\mathbf{j}$ on the same(different) sublattice.

Equal Time Correlations

The kinetic energy directly measures the effect of strain via an anisotropic hopping in the x and y directions. We will also display k_x/t_x and k_y/t_y to isolate the 'trivial' factor of the energy scales. Figure 4 shows the kinetic energies as functions of the hopping anisotropy δ. These evolve smoothly with δ, increasing in the $\hat{y}$ direction for which $t_y = 1+\delta$ and decreasing in the $\hat{x}$ direction where $t_x = 1-\delta$.

The real space density correlations $\langle \left(n_{\mathbf{i}\uparrow} + n_{\mathbf{i}\downarrow} \right) \left(n_{\mathbf{j}\uparrow} + n_{\mathbf{j}\downarrow} \right) \rangle$ are given in Figs. 5 and 6. For moderate anisotropy, $\delta = 0.5$, the correlations seem to extend over the entire lattice in a checkerboard pattern expected for (π,π) ordering. For large anisotropy, $\delta = 0.8$, the pattern is much reduced, especially in the $\hat{x}$ direction. Indeed, a pair of domain walls appears, across which the sublattices with high and low occupancy are reversed.

The CDW structure factor is sensitive to the development of long range change order. In the high temperature, disordered, phase $\langle \left(n_{\mathbf{i}\uparrow} + n_{\mathbf{i}\downarrow} \right) \left(n_{\mathbf{j}\uparrow} + n_{\mathbf{j}\downarrow} \right) \rangle$ is short ranged and $S_{\rm cdw}$ is independent of lattice size N. In the ordered phase $S_{\rm cdw}$ grows linearly with N. $S_{\rm cdw}$ is shown as a function of δ for different inverse temperatures β in Fig. 7

We do finite size scaling of $S_{\rm cdw}$ to identify T_c, a task that is considerably simplified by the knowledge that the appropriate universality class is that of the 2D Ising model, Insert some details. since CDW order breaks a two-fold discrete symmetry on our square lattice[21–23]. Results are shown for $\delta t = 0.4$ in Fig. 8. Insert some further discussion.

One might naively expect that T_c would scale as $t^2/U_{\rm eff}$, the scale which reflects the difference between a doubly occupied and empty site being adjacent relative to two doubly occupied or two empty sites. The kinetic energy measurement of Fig. 4 gives a sense of how this quantity varies in $\hat{x}$ direction. At $\delta = 0.5$ it is lower by a factor of roughly three, so that T_c might be expected to be reduced by an order of magnitude from $T_c \sim t/6$ in the isotropic case. This almost certainly underestimates T_c since it ignores the enhancement of density correlations in the $\hat{y}$ direction. Nevertheless these estimates seem consistent with the fact that CDW order is challenging to see at $\beta t = 24$, four times the isotropic β_c.

What other DQMC plots will we show?

Spectral Function

The spectral function can be obtained from the Greens function measurement in DQMC combined with analytic continuation[24] to invert the integral relation

$$G(\mathbf{p},\tau) = \int d\omega \frac{e^{-\omega\tau} A(\mathbf{p},\omega)}{e^{-\beta\omega}+1} \quad (6)$$

In the single site ($t_x = t_y = 0$) limit, the spectral function is temperature (and momentum) independent and consists of two delta-function peaks separated by $U_{\rm eff}$,

$$A(\mathbf{p},\omega) = \frac{1}{2}\Big(\delta(\omega + \frac{\lambda^2}{2\,\omega_0^2}) + \delta(\omega - \frac{\lambda^2}{2\,\omega_0^2}) \Big) \quad (7)$$

The density of states $N(\omega) = 1/N \sum_{\mathbf{p}} A(\mathbf{p},\omega)$.

Following the procedure discussed in [25] one can evaluate the moments

$$\mu_1(\mathbf{p}) \equiv \int d\omega\, \omega\, A(\mathbf{p},\omega) = \left(\epsilon_{\mathbf{p}} - \mu \right) + \lambda \langle X \rangle \quad (8)$$

$$\mu_2(\mathbf{p}) \equiv \int d\omega\, \omega^2\, A(\mathbf{p},\omega) = 4(1+\delta t^2)t^2 - \frac{\lambda^4}{\omega_0^4} + 2\frac{\lambda^4}{\omega_0^4}\langle \mathcal{P} \rangle$$

Here $\langle X \rangle$ is the phonon displacement on a spatial site, and is related to the density by $\langle X \rangle = x_* = -\lambda \langle n \rangle / \omega_0^2$. $\langle \mathcal{P} \rangle$ is the phonon potential energy. At half-filling, $\langle n \rangle = 1$ and $\mu = U_{\rm eff} = -\lambda^2/\omega_0^2$ so that $\mu_1(\mathbf{p}) = \epsilon_{\mathbf{p}}$. (This is the same as for the noninteracting case, since there $A(\mathbf{p},\omega) = \delta(\omega - \epsilon_{\mathbf{p}})$.) These analytic values of

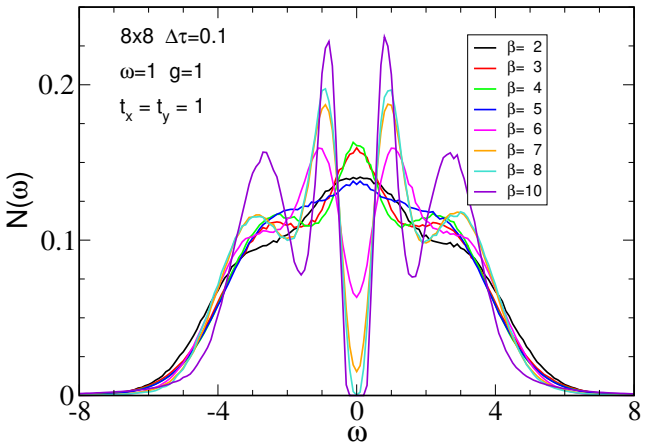

FIG. 9. Density of states for the isotropic lattice for different inverse temperatures β. The phonon frequency $\omega_0 = t$ and electron-phonon coupling $\lambda = \sqrt{2}\,t$. Finite size scaling of $S_{\rm cdw}$ suggests $\beta_c\,t = 6.0 \pm 0.1$ [26].

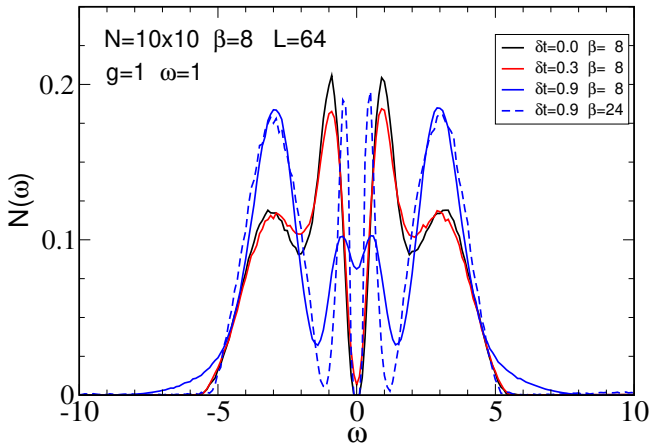

FIG. 10. Density of states comparing the isotropic lattice with small ($\delta = 0.3$) and large ($\delta = 0.9$) anisotropy. For $\delta = 0.9$ the opening of a gap is delated until $\beta_c\,t \sim 20$.

the moments, in combination with a measurement of the phonon potential energy, serve as a useful check on the analytic continuation.

This result needs to be checked. The second moments do not agree with what is coming out of Anders' maxent code.

Figure 9 shows the density of states $N(\omega)$ for the isotropic lattice. At inverse temperatures $\beta\,t = 2, 3, 4, 5$ lower than $\beta_c t$, $N(\omega)$ has a peak at the Fermi level $\omega = 0$. Beginning at the critical inverse temperature,

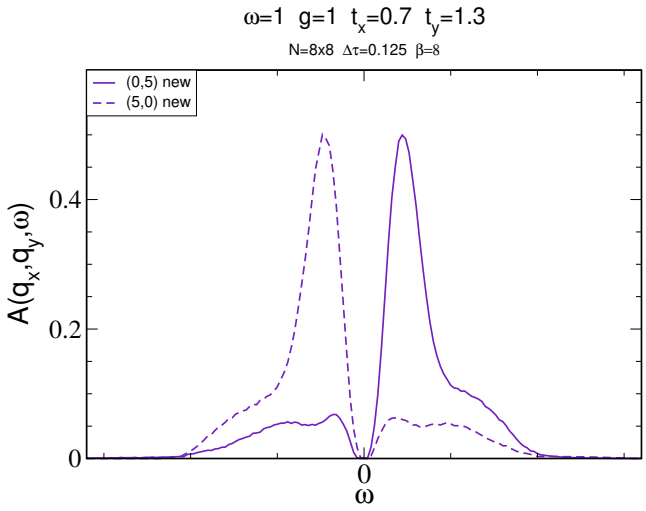

FIG. 11. A first attempt. Notice $A(p_x, p_y, \omega) = A(p_y, p_x, -\omega)$. Natanael saw this as well for dispersionful phonons. I do not understand it. I expected the peak in $A(5, 0, \omega)$ to be shifted closer to $\omega = 0$ than $A(0, 5, \omega)$ to reflect the smaller bandwidth in the x direction.

inferred finite size scaling of $S_{\rm cdw}$[26], $N(\omega)$ develops a gap which provides another indication of the transition to the insulating CDW phase. $N(\omega)$ remains relatively unchanged under the influence of strain $\delta t = 0.3$, Fig. , consistent with the robust $S_{\rm cdw}$ of 7 at modest anisotropy. However, at $\delta t = 0.9$ the CDW gap has been replaced by a weak minimum at $\beta\,t = 8$ and is only recovered at $\beta\,t = 24$.

While $N(\omega)$ gives information about the CDW gap, the momentum-resolved spectral function $A(\mathbf{p}, \omega)$ yields the effect of (strain) hopping anisotropy on the quasiparticle dispersion. Figure 11 shows $A(\mathbf{p}, \omega)$ versus ω) for several different points in the Brillouin zone. Actually, to make Figs. 11 and 12 more distinct, it might maks sense to show $A(\mathbf{p}, \omega)$ at fixed $\mathbf{p}$ and different δt in the former. Figure 11 exhibits the quasiparticle dispersion relation. Maybe it would be good to show several values $\delta t = 0.0, 0.3, 0.9$. If yes, Fig. 11 might just be superfluous.

Transition Temperature

Before presenting the results for the effect of anisotropy on the transition temperature T_c we recall the behavior of T_c for the related problem of the 2D Ising model with $J_x \neq J_y$. The Onsager solution is

(9)

Natanael or Ben- complete this discussion. That T_c is non-zero for all J_x/J_y is consistent with the general expectation that anisotropy in the form of a weak

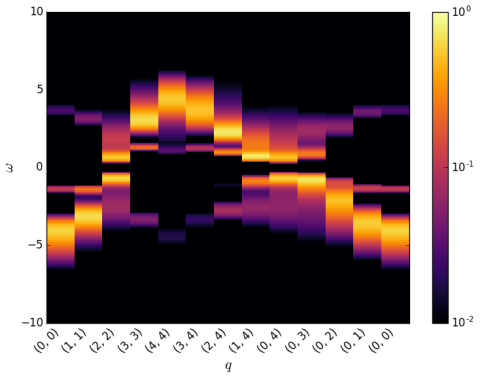

FIG. 12. This is an old figure of Natanael's for the dispersionful-phonon project. We want the analog for strain.

coupling in one direction does not destroy a finite temperature second order phase transition in dimension d. The rough physical picture is that correlations will develop in the 'strongly interacting' directions out to a length ξ. The coordinated orientation of degrees of freedom in regions of size ξ^{d-1} then create a large 'effective' coupling $J_{\rm eff} \sim \xi^{d-1} J_{\rm small}$ in the weakly interacting direction. As ξ grows $J_{\rm eff}$ eventually boosts $J_{\rm small}$. Our naive expectation, then, is that T_c for our 2D anisotropic Holstein model should be non-zero for all δ. This is substantiated by the MFT results of Fig. 3.

However, Fig. 7, however, would seem to cast doubt on a CDW transition at large strain. Even at $\beta t = 24$, $S_{\rm cdw}$ is less than 1/20 of its value for perfect (no quantum or thermal fluctuation) charge order. Iniitial insight into this is provided by the MFT treatment. From Fig. 2 we can infer the order parameter $x_1 \approx XX$. Since $S_{\rm cdw} \to N x_1^2$ in the thermodynamic limit we see MFT predicts this small value of the structure factor as a reflection of a small order parameter. The behavior of $N(\omega)$ provides more definitive evidence of the persistence of the CDW insulating phase even at high strain. Despite the small value of $S_{\rm cdw}$, the density of states has a clear gap at $\delta t = 0.9$ at low temperatures (Fig.).

CONCLUSIONS

While we have focussed here exclusively on using DQMC and MFT to understand the effects of anisotropic electron hopping $t_x \neq t_y$ on charge correlations and the gap in the Holstein model, it is also possible to examine the role of changes in the phonon spectra. Indeed, DFT calculations[2] indicate that such changes, e.g. enhancement of the phonon frequency with compression, are central to the onset of CDW order. Similarly, it is known from DQMC simulations that T_c exhibits a non-monotonic dependence on $\lambda_D = \lambda^2/(\omega_0^2 W)$ in the Holstein Hamiltonian[22]. However, the possibility of direct connection of such model calculations to materials would require the introduction of an ad hoc connection of ω_0 (and λ) to strain.

While applications of DQMC to Hamiltonians with repulsive electron-electron interactions are limited by the sign problem[19, 20], study of Holstein or Su-Schrieffer-Heeger models with electron-phonon interactions are much less restricted. As seen here, and in other work[21–23], low enough temperatures can be reached to get a complete understanding of the CDW transition, and even of the possibility of quantum critical points[22, 23] associated with CDW transitions driven by changes in λ_D at $T = 0$. Recent work has further exhibited this flexibility of DQMC by examining the effects of phonon dispersion on CDW order in the Holstein model[26]. In short, the freedom from the sign problem opens the door to incorporating additional materials details into quantum simulations of electron-phonon models and hence to the study of CDW transitions. Such rich details are much more difficult to include in studies of repulsive electron-electron interactions like the Hubbard model for which the sign problem is severe.

Acknowledgements: The work of B. C-S. and R.T.S. was supported by the Department of Energy under grant DE-SC0014671. N.C.C. was supported by the Brazilian funding agencies CAPES and CNPq. Ehsan NSF.

* bwcohenstead@ucdavis.edu

[1] L. Gan, L. Zhang, Q. Zhang, C. Guo, U. Schwingenschlogl, and Y. Zhao, Phys. Chem. Chem. Phys. **18**, 3080 (2016).
[2] M. J. Wei, W. J. Lu, R. C. Xiao, H. Y. Lv, P. Tong, W. H. Song, and Y. P. Sun, Phys. Rev. B **96**, 165404 (2017).
[3] S. Gao, F. Flicker, R. Sankar, H. Zhao, Z. Ren, B. Rachmilowitz, S. Balachandar, F. Chou, K. S. Burch, Z. Wang, J. van Wezel, and I. Zeljkovic, Proc. Nat. Acad. Sci. **115**, 6986 (2018), https://www.pnas.org/content/115/27/6986.full.pdf.
[4] M. D. Johannes, I. I. Mazin, and C. A. Howells, Phys. Rev. B **73**, 205102 (2006).
[5] M. D. Johannes and I. I. Mazin, Phys. Rev. B **77**, 165135 (2008).
[6] A. Tsen, R. Hovden, D. Wang, Y. Kim, J. Okamoto, K. Spoth, Y. Liu, W. Lu, Y. Sun, J. Hone, L. Kourkoutis, P. Kim, and A. Pasupathy, Proceedings of the National Academy of Sciences **112**, 15054 (2015), https://www.pnas.org/content/112/49/15054.full.pdf.
[7] J. Yang, W. Wang, Y. Liu, H. Du, W. Ning, G. Zheng, C. Jin, Y. Han, N. Wang, Z. Yang, M. Tian, and Y. Zhang, Appl. Phys. Lett. **105**, 063109 (2014).
[8] J. Renteria, R. Samnakay, C. Jiang, T. Pope, P. Goli, Z.Yan, D. Wickramaratne, T. Salguero, A. Khitun, R. Lake, and A. Balandin, J. Appl. Phys. **115**, 034305 (2014).
[9] Y. Yu, F. Yang, X. Lu, Y. Yan, Y. Cho, L. Ma, X. Niu,

S. Kim, Y. Son, D. Feng, S. Li, S. Cheong, X. Chen, and Z. Y., Nat. Nanotechnol. **10**, 270 (2015).
[10] M. Hollander, Y. Liu, W. Lu, L. Li, Y. Sun, J. Robinson, and S. Datta, Nano Lett. **15**, 1861 (2015).
[11] R. Samnakay, D. Wickramaratne, T. Pope, R. Lake, T. Salguero, and A. Balandin, Nano Lett. **15**, 2965 (2015).
[12] X. Xi, L. Zhao, Z. Wang, H. Berger, L. Forró, J. Shan, , and K. Mak, Nat. Nanotech. **10**, 765 (2015).
[13] P. Chen, Y. H. Chan, X. Fang, Y. Zhang, M. Y. Chou, S. K. Mo, Z. Hussain, A. V. Fedorov, and T. C. Chiang, Nat. Comm. **6**, 8943 (2015).
[14] P. Chen, Y. Chan, M. Wong, X. Fang, M. Chou, S. Mo, Z. Hussain, A. Fedorov, and T. Chiang, Nano Lett. **16**, 6331 (2016).
[15] C. Lian, C. Si, J. Wu, and W. Duan, Phys. Rev. B **96**, 235426 (2017).
[16] D. Zhang, J. Ha, H. Baek, Y.-H. Chan, F. D. Natterer, A. F. Myers, J. D. Schumacher, W. G. Cullen, A. V. Davydov, Y. Kuk, M. Y. Chou, N. B. Zhitenev, and J. A. Stroscio, Phys. Rev. Materials **1**, 024005 (2017).
[17] T. Holstein, Annals of Physics **8**, 325 (1959).
[18] W. Su, J. Schrieffer, and A. Heeger, Phys. Rev. Lett. **42**, 1698 (1979).
[19] E. Loh, J. Gubernatis, R. Scalettar, S. White, D. Scalapino, and R. Sugar, Phys. Rev. B **41**, 9301 (1990).
[20] M. Troyer and U. Wiese, Phys. Rev. Lett. **94**, 170201 (2005).
[21] M. Weber and M. Hohenadler, Phys. Rev. B **98**, 085405 (2018).
[22] X. Zhang, W. Chiu, N. Costa, G. Batrouni, and R. Scalettar, axXiv:1809.07902.
[23] C. Chen, X. Xu, Z. Meng, and M. Hohenadler, axXiv:1809.07903.
[24] M. Jarrell and J.E.Gubernatis, Physics Reports **269**, 133 (1996).
[25] S. White, Phys. Rev. B **44**, 4670 (1991).
[26] N. C. Costa, T. Blommel, W.-T. Chiu, G. Batrouni, and R. T. Scalettar, Phys. Rev. Lett. **120**, 187003 (2018).

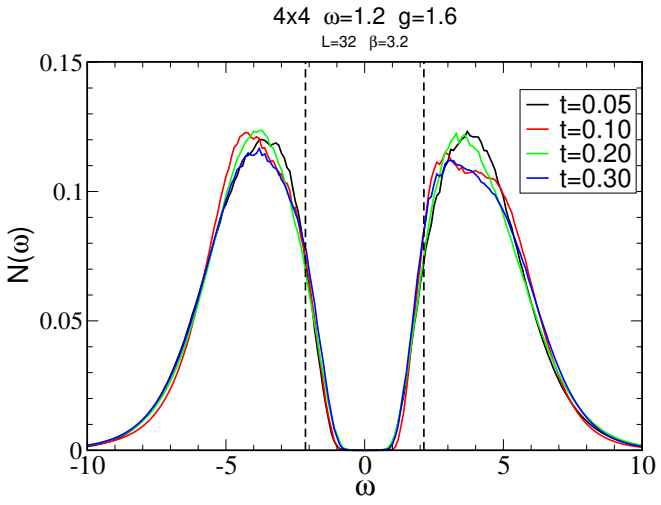

FIG. 13. Density of states for small t. It does not seem to match the analytic $t = 0$ form which implies two delta function peaks at $\omega = \pm\lambda^2/\omega^2$.

SUPPLEMENTAL MATERIALS

Placing some additional results here for further analysis later.

Figure 13 is a check of the $t = 0$ result for the spectral function

$$A(\omega) = \frac{1}{2}\big(\delta(\omega + \frac{\lambda^2}{2\,\omega_0^2}) + \delta(\omega - \frac{\lambda^2}{2\,\omega_0^2})\ \big) \qquad (10)$$

Do I have a factor of two wrong? The DQMC results peaks are twice as far from the origin as the exact expression. On the other hand, I like the fact that the peaks are separated by $U_{\rm eff}$ since for the Hubbard model they are separated by U. Ben should check.